Integrative Biology

Accepted Manuscript

This is an *Accepted Manuscript*, which has been through the Royal Society of Chemistry peer review process and has been accepted for publication.

Accepted Manuscripts are published online shortly after acceptance, before technical editing, formatting and proof reading. Using this free service, authors can make their results available to the community, in citable form, before we publish the edited article. We will replace this *Accepted Manuscript* with the edited and formatted *Advance Article* as soon as it is available.

You can find more information about *Accepted Manuscripts* in the Information for Authors.

Please note that technical editing may introduce minor changes to the text and/or graphics, which may alter content. The journal's standard Terms & Conditions and the Ethical guidelines still apply. In no event shall the Royal Society of Chemistry be held responsible for any errors or omissions in this *Accepted Manuscript* or any consequences arising from the use of any information it contains.

ROYAL SOCIETY OF CHEMISTRY

www.rsc.org/ibiology

Graphical Abstract

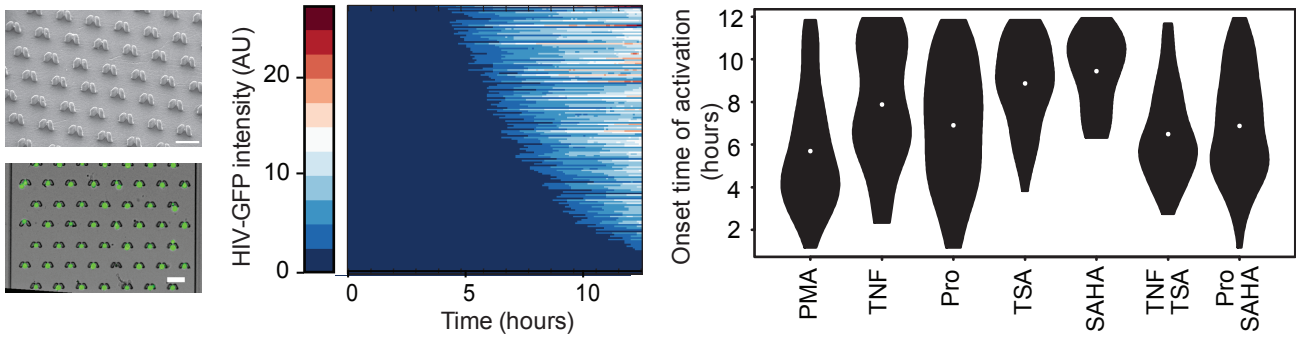

We designed a passive-flow microfluidic device to image HIV activation dynamics in live individual T cells. We show that drugs that activiate transcription factors stimulate latent HIV with distinct noise profiles from drugs that inhibit chromatin remodeling proteins.

Integrative Biology Accepted Manuscript

Insight, Innovation, Integration

Noisy viral reactivation in response to drug stimulation presents an obstacle to purging latent HIV from infected T cells in a clinical setting. To measure variability in latent HIV activation, we designed a passive-flow microfluidic device to image viral activation dynamics in single T cells. We observed that the onset of viral expression and rate of HIV production are independently regulated in single cells. We further found that histone deacetylase inhibitors stimulated more uniform onset times, while drugs activating the nuclear factor-κB transcription factor (TF) via protein kinase C exhibited more variation in activation rates. Our results suggest that variation in viral activation should be considered when optimizing therapeutic anti-latency strategies. Overall, our device presents a useful tool for implementing live-cell imaging protocols in suspension cells.

Integrative Biology Accepted Manuscript

A passive-flow microfluidic device for imaging latent HIV activation dynamics in single T cells

Ramesh Ramji,*[a] Victor C. Wong,*[b] Arvind K. Chavali,*[a] Larisa M. Gearhart,[a,c] Kathryn Miller-Jensen[a,b]

Abstract

Quantifying cell-to-cell variability in drug response dynamics is important when evaluating therapeutic efficacy. For example, optimizing latency reversing agents (LRAs) for use in a clinical "activate-and-kill" strategy to purge the latent HIV reservoir in patients requires minimizing heterogeneous viral activation dynamics. To evaluate how heterogeneity in latent HIV activation varies across a range of LRAs, we tracked drug-induced response dynamics in single cells via live-cell imaging using a latent HIV–GFP reporter virus in a clonal Jurkat T cell line. To enable these studies in suspension cells, we designed a simple method to capture an array of single Jurkat T cells using a passive-flow microfluidic device. Our device, which does not require external pumps or tubing, can trap hundreds of cells within minutes with a high retention rate over 12 hours of imaging. Using this device, we quantified heterogeneity in viral activation stimulated by transcription factor (TF) activators and histone deacetylase (HDAC) inhibitors. Generally, TF activators resulted in both faster onset of viral activation and faster rates of production, while HDAC inhibitors resulted in more uniform onset times, but more heterogeneous rates of production. Finally, we demonstrated that while onset time of viral gene expression and rate of viral production together predict total HIV activation, rate and onset time were not correlated within the same individual cell, suggesting that these features are regulated independently. Overall, our results reveal drug-specific patterns of noisy HIV activation dynamics not previously identified in static single-cell assays, which may require consideration for the most effective activate-and-kill regime.

Integrative Biology Accepted Manuscript

Introduction

Genetically identical cells often exhibit heterogeneous behaviors in response to homogeneous stimuli due to variable concentrations of intracellular factors and fluctuations in biochemical reactions. In some cases, this biological noise is advantageous for the survival and propagation of an organism. For example, diversity in protein levels across a clonal population of *E. coli* can ensure rapid adaptability to a changing environment [1, 2]. However, non-genetic variability in response to drug treatment undermines therapeutic efficacy. Biological noise gives rise to bacterial "persister" cells that can survive antibiotic treatment [3] and "fractional killing" by chemotherapeutics can limit the effectiveness of cancer therapy [4].

Recently, heterogeneous reactivation of latent HIV proviruses in response to latency reversing agents (LRAs) has emerged as a challenge to the "activate-and-kill" strategy to purge the latent reservoir from infected patients [5, 6]. Latent HIV infections are transcriptionally silent and therefore invisible to antiretroviral therapies and the host immune system. One promising therapeutic strategy is to purge the latent cellular reservoir by systematically reactivating latent HIV with LRAs [7-9]. However, both entry and exit from viral latency is largely a probabilistic process that depends on heterogeneity in host factors, as well as stochasticity inherent to the HIV promoter [10-13]. Although the molecular basis of stochasticity in HIV latency was originally established in T cell lines, recent findings suggest that reactivation of latent HIV proviruses in resting CD4+ T cells isolated from patients is also intrinsically stochastic [5]. Together, these observations suggest that understanding the dynamics and sources of noise in HIV reactivation will be necessary to optimize an LRA stimulation strategy that will completely clear the viral reservoir [14, 15].

The preclinical efficacy of LRAs is generally determined by stimulating latent virus reactivation in either Jurkat T cell lines or primary T cell latency models containing HIV reporters, and then assessing the final fraction and/or expression level of activated virus. However, this traditional method of drug screening does not capture cell-to-cell variability in the dynamics of activation that may be important for evaluating drug efficacy. Long-term time-lapse imaging is the best way to collect dynamic activation data; however, the non-adherent nature of T cells makes this approach difficult in tissue culture plates unless cells are immobilized with a surface modification such as poly-lysine, which may affect cell response. Therefore, we sought to develop an easy and efficient method to immobilize and stimulate suspension cells over long durations, while maintaining the simplicity of plate-based approaches. Such a device would enable quantitative measurements of LRA-stimulated HIV reactivation over time in single cells.

Microwell-based cell docking procedures have been reported for yeast and mammalian cells [16-18], but most of these methods rely on gravity to capture cells and therefore cells are easily dislodged when changing chemical or biological solutions because cells are not actively held in the wells [19]. Methods that use hydrodynamic flow focusing work better in terms of sequential and deterministic trapping of cells, while also

Integrative Biology Accepted Manuscript

permitting delivery of various chemical or biological stimuli with minimal shear [20, 21]. For example, a microfluidic device that uses hydrodynamic flow to capture single cells in a high density array was used to monitor calcium oscillatory behavior in Jurkat T cells [13, 19]. Such hydrodynamic flow focusing methods require pressure-based pumping, in which syringe pumps or tubing placed at different heights control the rate of fluid flow within the channel. However, connecting tubing can change the pressure inside the device and is not compatible with some environmental chambers or microscope stage incubators used for live-cell imaging.

To simplify cell loading and on-chip stimulations, we designed a microfluidic device that operates based on passive flow (i.e., without tubing) in order to dock cells in an array within a few minutes and retain them over many hours, while also permitting fast exchange of solutions during stimulation. We used our device to carry out time-lapse HIV reactivation assays on a Jurkat T cell HIV latency model [22] using two classes of LRAs: transcription factor (TF) activators and histone deacetylase (HDAC) inhibitors. By quantifying activation dynamics at a single-cell level, we were able to measure heterogeneity in dynamic responses to drugs that could not be quantified using a conventional flow cytometry-based assay. In general, TF activators stimulated a faster onset of activation time and greater rate of HIV production, while HDAC inhibitors were more heterogeneous in terms of expression but with more uniform onset times. Our data suggest that separate mechanisms underlie the onset time of activation and the rate of HIV production in single cells, and that individual LRAs differentially affect these mechanisms to achieve HIV activation. Overall, our study demonstrates that targeting unique latency regulatory pathways results in significant differences in reactivation noise and reveals a potential limitation to the effectiveness of the activate-and-kill strategy.

Results

Design and optimization of a passive-flow microfluidic device for cell trapping and live-cell imaging

Time-lapse imaging of Jurkat T cells is usually achieved by immobilizing cells via a cell surface modification. In addition to possibly perturbing the physiology of the cells, in some cases these modifications are not enough to fully restrict cell movement over multiple hours. For example, phorbol 12-myristate 13-acetate (PMA) is a potent activator of HIV transcription in both cell line HIV latency models and patient samples, and is therefore considered a benchmark for evaluating LRA efficacy [23, 24]. However, PMA stimulation makes Jurkat T cells highly motile even in the presence of poly-lysine, making it difficult to image activation in live cells (Movie S1). In addition to long-term immobilization of cells, we also required a device that 1) could be placed inside a microscope stage incubator without external tubing; 2) would allow fast exchange of solutions to rapidly stimulate the cells without displacing them; and 3) would permit screening of multiple drugs across several parallel experiments.

Integrative Biology Accepted Manuscript

To address our needs, we designed a microfluidic device that can capture single cells in an array without using pumps or tubing to aid in fluid flow within the device. The passive-flow microfluidic device consists of physical traps embedded in a center channel, connecting an inlet and an outlet reservoir (Fig. 1A). Fluid flow through the channel is achieved by altering the surface wettability of the channel. Treating the glass surface and the inner walls of the PDMS microchannel with oxygen plasma introduces polar functional groups on PDMS, thus rendering the surface hydrophilic [25]. This step not only produces irreversible bonding of PDMS to glass but also reduces the contact angle of water to the PDMS surface, thereby allowing easy flow of fluid through the channel. By maintaining the channel with deionized water following plasma treatment, the channel will retain its hydrophilicity prior to cell loading. Cells are loaded into the inlet reservoir with a standard pipet, and cells are trapped as they passively flow from the inlet to the outlet. Cells that are not positioned in the traps can be washed away by replacing the cell solution at the inlet with plain media (Fig. 1B) thus capturing an array of single cells within the device.

To optimize capture of single suspension T cells with diameters ranging from 9-16 μm, we varied both trap design and trap density (Fig. 2A). The basic trap shapes included S-shaped square pillars (10 μm x 10 μm; S traps) and V-shaped rectangular pillars (10 μm x 7 μm; V traps), both with sides inclined at 30˚ and separated by a 5 μm gap (Fig. S1). We also tested two different trap densities by varying the column spacing between the traps. For the low-density traps, the horizontal spacing between traps for the S and V traps was 130 μm, while it was approximately 65 μm for the high-density traps (referred to as Hd-S and Hd-V traps). The vertical spacing between traps was approximately 55 μm for all four designs. The center channel connecting inlet and outlet reservoirs was 5.97 mm x 0.53 mm (length x width), resulting in 486 and 408 traps (S and V traps, respectively) for the low-density design, and 765 traps per device for the HD-S and HD-V designs.

Flow profiles for these four designs were simulated by solving a stationary Navier-Stokes equation with a shallow channel approximation. The surface and streamline plots demonstrate that the more closely packed Hd traps have a higher fluidic resistance between traps than the more widely spaced S and V trap designs (Fig. 2B). This analysis suggested that more densely packed traps would enable more efficient cell capture since the fluidic streamlines are compressed in a compact configuration in front of the high density traps, while for the low density traps, cells might be more easily diverted around the traps. Because a higher cell density is generally more favorable for imaging, we proceeded to optimize our protocol for the Hd traps.

To test the efficiency of capturing and retaining suspension cells directly using the passive-flow device, Jurkat T cells stained with calceinAM dye were perfused at different cell densities and flow volumes to measure the cell trapping efficiency. The overall trapping efficiency was calculated by counting all traps that contained *at least* one cell, while the single-cell trapping efficiency was calculated by counting only those traps that

Integrative Biology Accepted Manuscript

contained *exactly* one cell (Fig. 2C). Overall, we did not find significant differences between the Hd-S and Hd-V traps for capturing Jurkat T cells. Below we summarize the results for the Hd-V traps, which is the design we chose to use to conduct our stimulation experiments.

To test how cell density affected trapping efficiency, the volume of the cell solution at the inlet was fixed at 50 μL (i.e., fixed flow velocity) while the cell density was varied between 1, 2.5 and 5 million cells/ml. As cell density increased, the overall trapping efficiency for the Hd-V traps increased from 22% to 98% and the single-cell trapping efficiency increased from 20% to 80% (Fig. 3A). There was no significant difference in trapping efficiencies for any of the trap designs across all cell-loading densities, with 5 million cells/ml being the optimal loading density for all trap configurations (Fig. S2A-B). We also tested the effect of flow velocity on the trapping efficiency. Specifically, we increased the flow velocity by increasing the volume of cell solution at the inlet from 50 μL to 100 μL. Cell density was kept fixed at 5 million cells/ml. The overall trapping efficiency for the Hd-V traps was approximately 98% for both loading volumes, but the single-cell trapping efficiency dropped from 82% to 52% when the loading volume was increased (indicating that more traps contained two or more cells). We also measured a drop in single-cell trapping efficiency at the higher flow rate for the Hd-S traps but not for the S and V traps (Fig. S2E-G). Thus, a lower flow velocity is optimal for obtaining a single-cell array. We further note that we never observed any cell deformation using our optimized experimental conditions, suggesting that minimal shear forces act on the cells while in the traps. Overall, we were able to achieve a very high cell trapping efficiency with any trap configuration after optimizing cell-density and flow volumes.

Finally, we characterized aspects of the device that are critical for performing our experimental assays. We performed several wash steps on the cells and demonstrated that this results in little to no loss of trapped cells (Fig. 3C and Fig. S2). We also measured cell retention in the trap for up to ~24 hours. Although captured cells are gradually dislodged from the traps over time, approximately 70% of the cells remained in traps at 12 hours (Fig. 3D). In addition to cell division, specific characteristics of Jurkat cells, including drug-induced motility and a tendency to form cell clusters, contributed to cell displacement; therefore we expect that retention efficiency might be different for another cell type. To calculate the lag in drug exposure time between the inlet and outlet, we added a colored dye solution at the inlet and measured the velocity at which this travelled. All cells in the channel are exposed to a drug solution added at the inlet within 26-30 seconds (Fig. 3E and Movie S2). The cell loading time–or time it takes to fill all the traps in the channel using the optimized loading protocol–ranged from 2-3 minutes (Fig. 3F and Movie S3). In summary, our simple passive-flow microfluidic device design enabled rapid single-cell trapping, rapid cell stimulations on chip, and cell retention over long incubation periods (at least 12 hours), making it an ideal device to screen for heterogeneous activation dynamics in Jurkat models of HIV latency.

Integrative Biology Accepted Manuscript

Passive-flow microfluidic device facilitates quantification of heterogeneous HIV activation dynamics in response to drug stimulation

Having optimized the passive-flow device for long-term imaging of suspension cells, we used the device to measure single-cell heterogeneity in activation of HIV gene expression in a Jurkat T cell line model of HIV latency. Jurkat T cell line models of HIV latency have been critical for the discovery of many molecular mechanisms that underlie the establishment and maintenance of latency [22, 26-30]. Several latent HIV-infected clonal Jurkat cell lines have been established that contain the provirus integrated at the same genetic location in every cell in order to control for the effect of integration site on viral activation [22]. These stable clonal cell lines provide an ideal experimental model in which to study transcriptional noise and variability in the reactivation of latent HIV, because even after controlling for integration position, activation is highly heterogeneous and occurs on the time scale of hours [11, 28, 31].

We compared two classes of LRAs that activate latent HIV proviruses through different mechanisms: 1) activators of the transcription factor NF-κB, which binds to κB sites at the HIV promoter to initiate transcription, and 2) HDAC inhibitors that reverse repressive chromatin at the HIV promoter. TF activators included PMA and prostratin (both phorbol esters), and tumor necrosis factor (TNF). TNF acts primarily via inhibitor of κB kinase (IKK) to activate NF-κB, while PMA and prostratin are potent activators of the protein kinase C (PKC) pathway. PMA in particular has been shown to strongly induce HIV transcription in cell line models of latency and infected patient samples [23, 24]. HDAC inhibitors included trichostatin A (TSA) and suberanilohydroxamic acid (SAHA). Inhibition of HDACs leads to hyperacetylation of nucleosomes at the HIV promoter and transcriptional initiation. Importantly, SAHA (also known as vorinostat) has been tested in a translational clinical study for its effectiveness as an LRA [32].

To measure dynamic activation of latent HIV in response to LRAs in the passive-flow device, cells were first trapped and washed as described (see Methods). Six regions of interest were identified to cover the entire length of each channel, allowing us to image a total of 2520 traps across 4 such micro-devices (bonded to a single glass slide) within 2.5 minutes. Wash buffers were then removed and treatments were added to the inlet. For each region of interest, a phase contrast and fluorescent image was taken every 5 minutes for up to 24 hours (Fig. 4A). We report our live-cell tracking results at 12 hours, by which time a substantial majority of cells remain in the traps (Fig. 3D) and have started to express HIV–GFP.

Visually, it is immediately apparent that LRA perturbation results in highly heterogeneous activation kinetics, with some cells activating as early as 3 hours post stimulation while others remain silent even after 12 hours (Fig. 4A-B). The TF activators acting via PKC activated the largest percentage of cells of any single-agent treatment: PMA activated 54% of cells after 12 hours, while prostratin activated 43% (Fig. 4B and Fig. S3A). TNF and TSA had similar levels of activation after 12 hours (28% and 30%, respectively). Interestingly, a larger percentage of TNF-treated cells activated after 6

Integrative Biology Accepted Manuscript

hours of stimulation than TSA-treated cells (7% versus 3%; Fig. 4B and Fig. S3A). SAHA exhibited the weakest activation (10% at 12 hours). Co-drugging the cells with a TF activator and an HDAC inhibitor resulted in an additive increase in the fraction of cells responding (52% for TNF+TSA and 66% for prostratin+SAHA), similar to previous reports for this latency model [33]. To ensure that the constant flow in the device did not change cell response compared to a plate-based experiment, we validated our results by flow cytometry (Fig S3B). The percentage of cells activated in the passive-flow device was very similar to the percentage activated in a plate at 6, 12 and even ~24 hours, although the sample size at the ~24-hour time point in the passive flow device was relatively small (R=0.92; Fig. 4C).

Activation of the NF-κB transcription factor stimulates more heterogeneous activation onset times in latent HIV than inhibition of HDACs

Our motivation for conducting dynamic single-cell assays was to determine if there was information contained in these measurements that cannot be inferred from static single-cell distributions such as those measured by flow cytometry. In order to quantify differences in the activation dynamics of the latent provirus across different drug perturbations, we extracted features from the single-cell trajectories (Fig. 4B) to obtain five metrics of comparison (Fig. 4D): 1) onset time (t_{on}), 2) maximum fluorescence observed (F_{maxO}), 3) final fluorescence at 12 hours (F_{final}), 4) the area under the curve of the fluorescence trajectory (AUC), and 5) the slope of each trajectory. We hypothesized that these dynamic metrics might provide useful information about the mechanism of action of the different classes of LRAs, because in most cases, the single-cell distributions of these metrics across treatments were significantly different (Table S1).

We first compared the activation onset times for each cell that expressed virus in response to treatment. Variability in onset times is a challenge for purging the latent reservoir with LRAs since drug exposure may be limited *in vivo* [32, 34]. The distribution of t_{on} across treatments was visualized with violin plots, and the heterogeneity was measured by calculating the coefficient of variation (CV) (Fig. 5A-B). In general, the onset of HIV activation occurred faster but with more variability in cells that were stimulated with TF activators as compared to HDAC inhibitors. As expected, all TF activators had faster average t_{on} than the HDAC inhibitors (< 8 hours versus 9+ hours). PMA and prostratin, the TF activators that act via the PKC pathway, elicited the least uniform t_{on} (CV=0.42 and 0.46, respectively), while cells treated with TNF were slightly less noisy (CV=0.36). In contrast, cells treated with HDAC inhibitors activated more uniformly than cells treated with TF activators (CV=0.22 and 0.18, respectively). To confirm that a more uniform t_{on} was not an artifact of collecting data at 12 hours rather than 24 hours (during which time activation by HDAC inhibitors substantially increased), we tracked cells up to ~24 hours by quantifying all cells that remained in the frame of view within the passive-flow device (to offset cell loss, Fig. 3D). We observed increased noise in t_{on} for all drugs, but the HDAC inhibitors still had more uniform t_{on} than the TF

Integrative Biology Accepted Manuscript

activators (Fig. S4), suggesting that a coordinated onset of activation is characteristic of the shared mechanism of action.

In other experimental systems, the transcription of some genes exhibits dependence on cell cycle [35, 36]. To preclude the possibility that heterogeneity in cell cycle stage contributes to the heterogeneity we observe in t_{on}, we synchronized cells via serum starvation for 24 hours and then quantified cell-to-cell variability in activation dynamics after 12 hours of PMA stimulation (Fig. S5). We observed similar CVs for t_{on} for cells synchronized prior to treatment versus cells that were not synchronized (Fig. S5A), suggesting that differences in cell cycle state are not substantially contributing to variability in the timing of reactivation.

Notably, dynamic cell responses revealed differences in drug classes that were not apparent by static assays. For example, TNF alone or TSA alone both activated a similar fraction of cells by 12 hours as measured in the device or by flow cytometry (Fig. S3). However, the dynamic single-cell activation data demonstrated that TSA produced a later but more uniform t_{on} that is consistent with a distinct mechanism of activation for TNF versus TSA.

Many studies of HIV latency activation, including results from patient cells, have suggested that co-drugging may be necessary to maximally purge the latent reservoir [33, 37-39]. Therefore, we next compared how co-drugging with HDAC inhibitors would affect variability in t_{on} for TF activators. When co-drugged with TNF and TSA, HIV activated with an earlier t_{on} more similar to PMA, but also reduced variability in t_{on} relative to stimulating with TNF or PMA alone (Fig. 5B). Co-drugging cells with prostratin and SAHA had little effect on mean t_{on} but resulted in less noise than treating with prostratin alone (Fig. 5B). These data suggest that co-drugging cells with a TF activator and HDAC inhibitor results in an earlier t_{on} while also lowering noise the onset of activation. Importantly, dynamic information about activation, such as variability in onset time, goes undetected in endpoint assays like flow cytometry but can provide critical information for the development of an effective LRA regime.

The rate of HIV production and the maximum level of HIV expression are less variable in response to TF activation versus inhibition of HDACs

The overall therapeutic objective of reactivating latent HIV via LRAs is to purge the latent reservoir by initiating replicative gene expression in the infected cells that results in cell death by cytotoxicity and/or clearance by the host immune system [40]. Recent observations suggest that there is a threshold of HIV particles that must be reached before active replication can be achieved [39] along with full potential for recognition by host cytotoxic T cells [40]. Therefore, in addition to measuring the onset of activation, quantifying cell-to-cell variability in gene expression levels is also important. We approximated abundance of gene expression by measuring the fluorescence intensity expressed by cells. We identified three metrics from the activation trajectories that represent HIV expression levels (F_{maxO}, F_{final}, and AUC; Fig. 4D). The

Integrative Biology Accepted Manuscript

values for these metrics were highly correlated across all treatments (compare Fig. 5C-D and Fig. S6), and therefore we chose F_{maxO} to approximate maximum HIV expression. By quantifying the change in expression over time, we were also able to determine the rate of HIV production (i.e., slope; Fig. 5E-F).

On average, TF activators stimulated greater mean HIV expression than HDAC inhibitors (Fig. 5C). PMA resulted in the largest F_{maxO}, followed by prostratin and TNF. While TSA-treated cells exhibited only slightly weaker HIV expression than TNF, SAHA-treated cells stimulated significantly lower levels of HIV. Treatments resulting in greater F_{maxO} also demonstrated more uniform levels of activation over 12 hours (Fig. 5D). Interestingly, PMA and prostratin had relatively low noise in F_{maxO} compared to TNF (CV=1.2 and 1.5 versus CV=2.2). TSA exhibited variability similar to TNF, while activation by SAHA was considerably more heterogeneous (Fig. 5D). The greater noise in F_{maxO} in response to HDAC inhibitors was in contrast to the lower noise in t_{on} (compare Fig. 5B and D).

Rates of HIV production showed identical trends. PMA and prostratin, which produced the strongest and most uniform HIV expression levels, also elicited the most rapid and uniform rates of HIV production (Fig. 5E-F; CV = 1.1-1.3). TNF and TSA stimulated similar variability in slope (CV=1.8-1.9) while SAHA had the highest variability (CV=3.4). As with onset time, variability between cell cycle synchronized and unsynchronized cells for F_{maxO} and slope were nearly identical after PMA treatment (Fig. S5B-C). Overall, we observed more uniform rates and levels of HIV activation in response to TF activators as compared to HDAC inhibitors in this T cell line model of latency.

Co-drugging with a TF activator and an HDAC inhibitor significantly decreased noise in both F_{maxO} and slope. For both cases of co-drugging, cells exhibited F_{maxO} distributions more similar to PMA-treated cells. These data again suggest that co-drugging may be beneficial in the clinic both by increasing the fraction of the reservoir that is activated and by decreasing the variability in the rate of HIV production, a result not previously identified in static assays.

Comparing the onset time of activation and the rate of HIV production in the same single cells suggests independent control mechanisms

The difference in noise between the t_{on} and noise in slope suggested that these two metrics may be differentially regulated (i.e. the onset of activation is not related to the rate of HIV production and vice versa). To examine this possibility, we calculated the correlation between t_{on} versus slope for all individual cells that reactivated in response to each treatment (Fig. 6A-B). Indeed, the correlation (R) between t_{on} and slope ranged from almost no correlation in the case of prostratin to a weak correlation in the case of SAHA (Fig. 6B). These data suggest that the onset of activation and the rate of HIV production are controlled by different biological mechanisms that are generally independent even within the same cell.

Integrative Biology Accepted Manuscript

Although t_{on} and slope are uncorrelated, each individual metric is correlated to total HIV abundance after 12 hours of stimulation (F_{maxO}; Fig. 6C). Multiple linear regression analysis confirmed that these two metrics are predictive of F_{maxO}, but that the extent to which t_{on} and slope contributed to F_{maxO} changed depending on the perturbation (Fig. 6D). Specifically, we calculated the regression coefficients for t_{on} and slope in predicting F_{maxO} separately for each LRA treatment in order to determine the amount of variation in F_{maxO} that can be explained by either the t_{on} or slope in a regression model. In all single-agent treatments except for prostratin, t_{on} and slope equally contributed to the variability in F_{maxO}. Under prostratin treatment, t_{on} was more predictive of F_{maxO}. Interestingly, however, when TF activators and HDAC inhibitors were combined, slope was slightly more predictive of F_{maxO}. These data suggest that co-drugging the latent virus with a TF activator and an HDAC inhibitor coordinates the mechanisms regulating t_{on} more than the mechanisms regulating slope. Consequently, the variability in slope is a greater determinant of the variability in F_{maxO}. To further reduce variability and improve treatment efficacy, a drug that preferentially affects the rate of HIV activation (e.g., a higher dose of prostratin) may be required.

Discussion

Understanding drug response dynamics and how they vary cell to cell is an important component to therapeutic efficacy, including the efficacy of LRAs in reversing HIV latency. An effective approach to investigate cell-to-cell response heterogeneity is to perform time-lapse imaging with a live-cell phenotypic reporter. To study activation of latent HIV, we used Jurkat CD4+ T cells that were clonally infected with an HIV reporter in order to control for integration site, while studying activation in a physiologically relevant cell type. By quantifying latent HIV activation in response to TF activators and HDAC inhibitors in live, single cells, we identified informative dynamic metrics that cannot be measured in static assays (Fig. 4). Specifically, in addition to quantifying the maximum activation of HIV in response to 12 hours of LRA stimulation, we also quantified the onset time of activation and the rate of HIV production. We detected significant cell-to-cell variability in these dynamic metrics, and we further demonstrated that perturbations have a differential effect on heterogeneity of these two metrics (Fig. 5). In general, HDAC inhibitors elicited slower, but less heterogeneous, onset time of activation than TF activators, while the TF activators stimulated greater and more uniform rates of production and maximum HIV expression levels.

Key to our study was the development of a novel, user-friendly microfluidic device to dock single suspension cells for long-term imaging analysis. Imaging suspension cells, such as Jurkat cells, is difficult because they do not adhere to cell surfaces without perturbing their biology through the use of a surface modification. Existing microfluidic cell-trapping methods designed to immobilize suspension cells require syringe pumps and tubing to alter flow within the microchannel. In contrast, our device uses passive flow by altering the surface hydrophilicity and volume differences

Integrative Biology Accepted Manuscript

across the device. Cells in suspension are loaded using a standard pipette into the inlet reservoir of the device, and cells are trapped by an array of microstructures in the center channel (Fig. 1). We specifically designed these traps to immobilize Jurkat T cells (9-16μm in diameter), but the traps can be resized to accommodate other cell diameters. Our device enables rapid cell loading (2-3 minutes), high trapping efficiency, and rapid on-chip stimulation (Fig. 3). The lack of pumps and tubing simplifies operation of the device by making it easy to place it into an environmental chamber for live-cell imaging, and to perform multiple experiments at the same. We anticipate that this device could be useful for imaging other suspension cells, including other immune cells and yeast.

Our results provide new information that may be relevant to evaluating the efficacy of clinical LRAs. For example, SAHA treatment, which presented promising results *in vivo* as a potentially effective LRA [32] resulted in both the lowest and most variable rate of HIV production and maximum expression. Because the bioavailability of any compound is limited *in vivo*, variability in activation presents an additional barrier to completely purging the latent HIV pool. The stochastic activation of latent HIV observed in patient samples suggests that LRAs that do not stimulate a rapid, uniform response will reactivate only a fraction of the latent reservoir, sparing enough cells to re-establish an active infection after the cessation of antiretroviral therapy. Due to the significant activation noise we observed in response to SAHA (Fig. 5C), we conclude that SAHA on its own is unlikely to elicit a response that is uniformly strong enough to effectively purge the latent reservoir. In contrast to SAHA, PMA is a potent activator of latent HIV across many latency models and in patient samples [23, 24], although it is not a viable option for therapy. We also observed that PMA was the strongest activator of HIV, and further observed that it produced relatively low noise in rate of HIV production. Interestingly, however, the onset times were more heterogeneous than for other treatments (Fig. 5B), demonstrating that even potent LRAs may be limited by variable response dynamics.

Several HIV latency studies have concluded that co-drugging cells with a TF activator and an HDAC inhibitor may be an effective way to improve LRA efficacy [37, 41]. We demonstrated that co-drugging cells increases overall activation by enhancing both onset time of activation and the rate of HIV production (Fig. 5). Additionally, we observed that co-drugging cells decreases heterogeneity in the rate and maximum level of HIV production. Previous observations based on static measurements have suggested that single treatments are sufficient to effectively reactivate HIV integrated into permissive chromatin environments [33]. However, our dynamic single-cell data suggest that co-drugging will always be more effective in activating latent HIV, because it stimulates not only a stronger and more rapid response, but also lowers response variability. Our results are consistent with recent findings that combinations of cancer therapeutics can be used to tune cell-to-cell variability in the timing and probability of cell death [42], suggesting that co-drugging may be a more general approach to reduce therapeutic response variability. Unequivocally

Integrative Biology Accepted Manuscript

Importantly, our study demonstrated that dynamic single-cell measurements provide information about underlying regulatory mechanisms. By comparing two dynamic metrics that contribute to total activation–onset time and the rate of HIV activation–in the same single cell, we demonstrated that these two features are generally not correlated within cells in response to most drug stimulations (Fig. 6C). This suggests that the biological mechanisms that regulate onset time and rate of HIV production are independent. Nucleosomes positioned at the HIV promoter contribute to latency maintenance [26, 27, 43, 44] by effectively setting a threshold for HIV activation that must be exceeded before viral expression can proceed [28]. Before the activation threshold is reached, the fluorescence marker for HIV production is undetectable, and therefore the onset of activation approximates this activation threshold that is regulated by nucleosomes and chromatin. In contrast, the rate of HIV production is regulated by the recruitment of the transcriptional machinery responsible for initiation and elongation and by the viral transactivator protein Tat [39, 45].

The poor correlation between the onset time of activation and the rate of HIV production in cells treated with TF activators is surprising given the dual role the NF-κB RelA:p50 heterodimer plays in the recruitment of both transcriptional machinery and histone acetyltransferases (HATs) to the HIV promoter. One possible explanation for this observation may be that the Tat protein decouples these roles by dramatically increasing elongation efficiency without significantly affecting chromatin structure. Another possibility is that there exists sufficient cell-to-cell heterogeneity in nucleosome occupancy [46, 47] and chromatin marks [48] such that the contribution NF-κB makes to activation onset time (via nucleosome/chromatin remodeling) and rate of HIV production appears to be uncorrelated from one cell to another. The observation that a weak correlation exists between onset time and production rate upon treatment with TSA and SAHA, which specifically target chromatin via HDACs, lend some support to the latter hypothesis.

The observation that the threshold of transcriptional activation and the rate of transcription are independently regulated within the same cell provides a different way to think about maximizing therapeutic efficacy, since both mechanisms influence maximum HIV expression. Multiple linear regression analysis demonstrates that while both the onset time of activation and the rate of HIV production contribute equally to the variability seen in maximum HIV expression for most single-agent treatments, they do not contribute equally when TF activators and HDAC inhibitors are combined. In this latency model, co-drugging resulted in a stronger correlation between the slope and maximum HIV expression, indicating that variability in maximum HIV expression is more dependent on the variability in rate of HIV production after co-drugging. This can be explained by considering the mechanisms of action of these drug classes. HDAC inhibitors primarily affect nucleosome stability, which reduces the variability in onset time by lowering the activation threshold across a population of cells. However, NF-κB RelA:p50 plays a role in transcriptional activation by recruiting transcriptional machinery and also recruiting HATs to the HIV promoter that target nucleosomes. NF-κB activation

Integrative Biology Accepted Manuscript

therefore creates an additive effect when combined with HDAC inhibitors, which further decreases the variability of onset time relative to the maximum HIV expression.

Given the growing observations that cell-to-cell variability affects biological responses in the immune system [49, 50], methods to facilitate live-cell imaging of suspension cells are critical. The passive-flow microfluidic device presented here enables a fast, simple, and effective means to capture suspension cells without changing their biology. For example, significant cell-to-cell variability is observed following chemotherapeutic treatments in adherent cancer cell lines [42, 51], but extended live-cell imaging has been limited in T cells and other immune cells because of the technical issues associated with immobilizing suspension cells. Therefore, this device would also be very useful in studying the kinetics of chemotherapeutic treatments for some lymphoma cells. In summary, we anticipate that the microfluidic device described here and the dynamic response data collected will be useful for studying biology in many types of suspension cells.

Experimental methods

Si Master Fabrication

The Si master containing different trap designs was etched using Oxford Plasmalab 100 Reactive ion etching system. Briefly, S1813 Microposit photoresist (Shipley) was spin coated at 900 rpm for 5 seconds and increased to 3000 rpm for 1 minute on a Si wafer. The photoresist coated wafer was baked on a hotplate at 100˚C for 3 minutes. The wafer was then removed from the hotplate and gradually cooled to room temperature while avoiding cooling blocks. The wafer was then exposed to 150 mJ/cm^2 UV light using EVG 620 contact/proximity mask aligner. A post exposure bake was carried out for 3 minutes at 120˚C. After this step, the wafer was cooled down to room temperature and developed in a Microposit MF-319 developer for 1 minute.

The developed master mold was then etched following a Bosch etch process resulting in a 20 μm feature height measured using a KLA-Tencor ASIQ profiler.

Microfluidic Device Fabrication

The etched master was silanized for 30 minutes inside a desiccator with Tricholoro(1H,1H,2H,2H-perfluorooctyl)silane (Sigma Aldrich) to prevent PDMS from sticking to it. Following this a mixture of PDMS (Sylgard 184 Elastomer kit, Dow Corning) base and curing agent 10:1 by weight, was mixed well and poured over the master placed on a plastic petri dish. This was degassed and cured for 2 hours at 75 ˚C. The cured PDMS mold was peeled from the master and cut to an appropriate size to fit the glass slide. A 7mm Harris Uni-Core puch (Ted Pella Inc.) was used to punch holes at the inlet and outlet ports to serve as reservoirs. The mold was then rinsed with Iso-propanol, blow dried with filtered air and scotch taped before plasma treatment. A standard 25 mm x 75 mm microscope glass slide cleaned in a similar way and placed

Integrative Biology Accepted Manuscript

inside a PE-25 benchtop plasma cleaner (Plasma Etch) along with PDMS molds. The glass slide and PDMS mold were exposed to O_2 plasma at 150W, 200 mTorr for 2 minutes and sandwiched immediately once removed from the plasma chamber. De-ionized water was used to fill the channels, the inlet and the outlet reservoirs in order to maintain the inner surface of the channels hydrophilic. This is an important step in making the device as there would be higher resistance for fluid flow when the inner walls of the microchannel are exposed to air leading to a hydrophobic recovery. Hence, it is recommended that the device is freshly prepared few hours before experiment while making sure that the device is filled with de-ionized water.

Cell line and culture conditions

Jurkat T cell clone J-Lat 10.6 obtained from NIH AIDS Research and Reference Reagent Program, Division of AIDS, NIAID, NIH was used for the HIV activation assays [22]. These cells were cultured in RPMI media 1640 supplemented with 10% fetal bovine serum, penicillin, streptomycin, L-glutamine and stored in an incubator at 37 ˚C and 5% CO_2. Cells were maintained at $2x10^5$ cells/mL and grown to log phase ($1x10^6$ cells/mL) before being loaded into microfluidic device for capture and activation. To synchronize the cells in the G_0 phase, cells were serum starved in RPMI media 1640 supplemented with penicillin, streptomycin, L-glutamine for 24 hours prior to stimulation with PMA.

Cell loading protocol

The cells were pelleted by centrifugation and re-suspended in fresh RPMI media 1640 while preparing them to be loaded into the microfluidic device. Cell clumps were dispersed immediately before loading by pipetting the cell suspension vigorously and filtering cells through a 35 μm nylon mesh strainer cap tube (BD Falcon). Cells were loaded into the inlet at volumes described in the results section and allowed to flow through the channel for 10 minutes. The cell suspension was then removed from the inlet by scrapping the bottom of the inlet reservoir with a pipette. Additional care should be taken to place the pipette tip opposite to the channel opening within the reservoir in order to avoid suction of trapped cells. Following this, 100 μL of wash liquid i.e. either RPMI media 1640 or Dulbecco's Phosphate-Buffered Saline (DPBS) was added to the inlet to wash the cells. Wash liquid was allowed to flow through the channel for 3 minutes which the liquid was again removed from outlet and inlet respectively. This wash procedure was repeated twice to remove any free floating cells from the main channel, inlet and outlet reservoirs and immediately followed by addition of either cell stimulants to the conduct the activation assay or RPMI media 1640 to perform further imaging and quantification of trapping efficiencies.

Cell stimulation

Prior to the addition of pharmacological agents, the microfluidic device was placed on the microscope stage and checked for optimal trapping efficiency. The wash liquid was then removed and replaced with a pharmacological agent by adding 150 μL of the solution to the inlet and 75 μL to the outlet, while the device remained on the microscope stage. The

Integrative Biology Accepted Manuscript

live-cell chamber was then sealed and imaging commenced (described below). The following treatments were used alone or in combination as described in the results section: 10 ng/mL tumor necrosis factor alpha (TNF) (Peprotech); 200 nM trichostatin A (TSA) and 10 nM phorbol 12-myristate 13-acetate (PMA) (Sigma-Aldrich); 4 μM prostratin and 4 μM SAHA (Santa Cruz Biotechnology).

Flow cytometry

Cells were plated at $5x10^5$ cells/mL in RPMI media 1640 and the previously listed pharmacological treatments were applied directly to the cells. Cells were fixed 0, 6, 12, and 24 hours after treatment in 4% formaldehyde. Cells were analyzed for HIV-GFP expression on an Accuri™ C6 Flow Cytometer (BD Biosciences).

Imaging

Images for the flow optimization experiments were captured using an EVOS FL Auto microscope. Both brightfield and fluorescent live cell stain Calcein-AM (Life technologies) images of cells were used for counting the number of cells trapped within the device. The cell simulation experiments were conducted on a Leica DMi8 widefield fluorescent microscope connected to an Andor iXon Ultra 897 EM-CCD camera. A 10X microscope objective was used to capture brightfield and green fluorescence images of HIV activation over a 14 hour time point. Adaptive focus control was set at each point to avoid any stage drifts during the course of long term imaging. The microfluidic device was placed on the microscope stage inside a TOKAI HIT live cell humidified chamber set to 37 ˚C and 5% CO_2.

Data Analysis

Flow optimization and cell stimulation images were processed in Image J and Imaris (Bitplane AG, Zurich, Switzerland), respectively. Images were background subtracted and a spot detection algorithm with a 16 μm spot diameter was used to detect and track the intensity change in reactivated cells. The number of non-reactivated cells caught in traps were counted manually from the bright field images. Each of the activated cells were assigned an identification number and stored in Microsoft Excel. A custom Perl (www.perl.org) script was used to organize the original raw data, which were subsequently passed through a series of filters accounting for the initial intensity value (to avoid counting basal activated cells), cut off time at 12 hours, smoothing of data (averaging 3 values for every data point), and cell displacement lengths. Unless otherwise stated, a cell displacement length of 5 μm was used in order to consider only the trapped cells and to avoid counting floating cells or cell passing the frame. Processed data from the Microsoft Excel file was used to calculate metrics such as area under the curve, coefficient of variation, maximum and final intensity, onset times, etc. Statistical analysis was performed in Prism (GraphPad Software, Inc., La Jolla, CA). Multiple linear regression was of the form

$$E(Y|X) = \alpha + \beta_1 X_1 + \beta_2 X_2$$

Integrative Biology Accepted Manuscript

where Y is F_{maxO}, X_1 is t_{on}, X_2 is S, α is the intercept, and β_j are the regression coefficients. Violin plots were generated with a custom script written in R (www.r-project.org).

Flow Simulation

Flow simulation for different trap designs was carried out in COMSOL Multiphysics (COMSOL Inc., Burlington, MA) using single phase laminar flow module. A fine mesh was generated for the entire subdomain with an automatic triangulation method. A PARDISO solver was used to solve the stationary Navier-Stokes equation using shallow channel approximation. An initial inlet velocity of 300 μm s^{-1} and outlet atmospheric pressure was used under no-slip boundary conditions. Surface plots representing flow velocity were plotted and compared with different trap designs.

Acknowledgements

We thank Vladimir Polejaev at the Yale West Campus Imaging Core for help with imaging. This work was supported by NSF grant CBET-1264246 and a Yale Dubinsky New Initiative grant (to K.M.J.). V.C.W. was supported by NIH Predoctoral Training Grants in Genetics (2T32GM007499-36, 5T32GM007499-34, 5T32GM007499-35). L.M.G. was supported by NSF grant DBI-1156585 and by the Raymond and Beverly Sackler Institute for Biological, Physical, and Engineering Sciences.

Notes

[a] Department of Biomedical Engineering, Yale University, New Haven, CT 06511
[b] Department of Molecular, Cellular, and Developmental Biology, Yale University, New Haven, CT 06511.
[c] Department of Biology, Mills College, Oakland, CA 94613
*These authors contributed equally to this work.

Electronic Supplementary Information (ESI) available. See DOI: 10.1039/b000000x/

References

1. Frankel, N.W., et al., *Adaptability of non-genetic diversity in bacterial chemotaxis.* eLIFE, 2014. **3**.
2. Losick, R. and C. Desplan, *Stochasticity and cell fate.* science, 2008. **320**(5872): p. 65-68.
3. Balaban, N.Q., et al., *Bacterial persistence as a phenotypic switch.* Science, 2004. **305**(5690): p. 1622-1625.

Integrative Biology Accepted Manuscript

4. Niepel, M., S.L. Spencer, and P.K. Sorger, *Non-genetic cell-to-cell variability and the consequences for pharmacology.* Current opinion in chemical biology, 2009. **13**(5): p. 556-561.
5. Ho, Y.-C., et al., *Replication-competent noninduced proviruses in the latent reservoir increase barrier to HIV-1 cure.* Cell, 2013. **155**(3): p. 540-551.
6. Rouzine, I.M., B.S. Razooky, and L.S. Weinberger, *Stochastic variability in HIV affects viral eradication.* Proceedings of the National Academy of Sciences, 2014. **111**(37): p. 13251-13252.
7. Biancotto, A., et al., *Dual role of prostratin in inhibition of infection and reactivation of human immunodeficiency virus from latency in primary blood lymphocytes and lymphoid tissue.* Journal of virology, 2004. **78**(19): p. 10507-10515.
8. Xing, S. and R.F. Siliciano, *Targeting HIV latency: pharmacologic strategies toward eradication.* Drug discovery today, 2013. **18**(11): p. 541-551.
9. Durand, C.M., J.N. Blankson, and R.F. Siliciano, *Developing strategies for HIV-1 eradication.* Trends in immunology, 2012. **33**(11): p. 554-562.
10. Weinberger, L.S., et al., *Stochastic gene expression in a lentiviral positive-feedback loop: HIV-1 Tat fluctuations drive phenotypic diversity.* Cell, 2005. **122**(2): p. 169-182.
11. Burnett, J.C., et al., *Control of stochastic gene expression by host factors at the HIV promoter.* PLoS pathogens, 2009. **5**(1): p. e1000260.
12. Miller-Jensen, K., et al., *Genetic selection for context-dependent stochastic phenotypes: Sp1 and TATA mutations increase phenotypic noise in HIV-1 gene expression.* PLoS computational biology, 2013. **9**(7): p. e1003135.
13. Razooky, B.S., et al., *A hardwired HIV latency program.* Cell, 2015. **160**(5): p. 990-1001.
14. Hill, A.L., et al., *Predicting the outcomes of treatment to eradicate the latent reservoir for HIV-1.* arXiv preprint arXiv:1403.4196, 2014.
15. Weinberger, A.D. and L.S. Weinberger, *Stochastic fate selection in HIV-infected patients.* Cell, 2013. **155**(3): p. 497-499.
16. Rettig, J.R. and A. Folch, *Large-scale single-cell trapping and imaging using microwell arrays.* Analytical chemistry, 2005. **77**(17): p. 5628-5634.
17. Park, M.C., et al., *High-throughput single-cell quantification using simple microwell-based cell docking and programmable time-course live-cell imaging.* Lab on a Chip, 2011. **11**(1): p. 79-86.
18. Park, J.Y., et al., *Single cell trapping in larger microwells capable of supporting cell spreading and proliferation.* Microfluidics and nanofluidics, 2010. **8**(2): p. 263-268.
19. Chung, K., et al., *Imaging single-cell signaling dynamics with a deterministic high-density single-cell trap array.* Analytical chemistry, 2011. **83**(18): p. 7044-7052.
20. Kobel, S., et al., *Optimization of microfluidic single cell trapping for long-term on-chip culture.* Lab on a Chip, 2010. **10**(7): p. 857-863.
21. Di Carlo, D., L.Y. Wu, and L.P. Lee, *Dynamic single cell culture array.* Lab on a Chip, 2006. **6**(11): p. 1445-1449.

Integrative Biology Accepted Manuscript

22. Jordan, A., D. Bisgrove, and E. Verdin, *HIV reproducibly establishes a latent infection after acute infection of T cells in vitro.* The EMBO journal, 2003. **22**(8): p. 1868-1877.
23. Spina, C.A., et al., *An in-depth comparison of latent HIV-1 reactivation in multiple cell model systems and resting CD4+ T cells from aviremic patients.* PLoS pathogens, 2013. **9**(12): p. e1003834.
24. Bullen, C.K., et al., *New ex vivo approaches distinguish effective and ineffective single agents for reversing HIV-1 latency in vivo.* Nature medicine, 2014. **20**(4): p. 425-429.
25. Tan, S.H., et al., *Oxygen plasma treatment for reducing hydrophobicity of a sealed polydimethylsiloxane microchannel.* Biomicrofluidics, 2010. **4**(3): p. 032204.
26. Rafati, H., et al., *Repressive LTR nucleosome positioning by the BAF complex is required for HIV latency.* PLoS biology, 2011. **9**(11): p. e1001206.
27. Williams, S.A., et al., *NF□κB p50 promotes HIV latency through HDAC recruitment and repression of transcriptional initiation.* The EMBO journal, 2006. **25**(1): p. 139-149.
28. Miller-Jensen, K., et al., *Chromatin accessibility at the HIV LTR promoter sets a threshold for NF-κB mediated viral gene expression.* Integrative Biology, 2012. **4**(6): p. 661-671.
29. Jordan, A., P. Defechereux, and E. Verdin, *The site of HIV□1 integration in the human genome determines basal transcriptional activity and response to Tat transactivation.* The EMBO journal, 2001. **20**(7): p. 1726-1738.
30. Kauder, S.E., et al., *Epigenetic regulation of HIV-1 latency by cytosine methylation.* PLoS pathogens, 2009. **5**(6): p. e1000495.
31. Weinberger, L.S., R.D. Dar, and M.L. Simpson, *Transient-mediated fate determination in a transcriptional circuit of HIV.* Nature genetics, 2008. **40**(4): p. 466-470.
32. Archin, N.M., et al., *Administration of vorinostat disrupts HIV-1 latency in patients on antiretroviral therapy.* Nature, 2012. **487**(7408): p. 482-485.
33. Wong, V.C., et al., *Quantitative Evaluation and Optimization of Co-drugging to Improve Anti-HIV Latency Therapy.* Cellular and Molecular Bioengineering, 2014. **7**(3): p. 320-333.
34. Archin, N.M., et al., *Expression of latent HIV induced by the potent HDAC inhibitor suberoylanilide hydroxamic acid.* AIDS research and human retroviruses, 2009. **25**(2): p. 207-212.
35. Zopf, C.J., et al., *Cell-cycle dependence of transcription dominates noise in gene expression.* PLoS computational biology, 2013. **9**(7): p. e1003161.
36. Padovan-Merhar, O., et al., *Single Mammalian Cells Compensate for Differences in Cellular Volume and DNA Copy Number through Independent Global Transcriptional Mechanisms.* Mol Cell, 2015. **58**(2): p. 339-52.
37. Reuse, S., et al., *Synergistic activation of HIV-1 expression by deacetylase inhibitors and prostratin: implications for treatment of latent infection.* PloS one, 2009. **4**(6): p. e6093.
38. Quivy, V., et al., *Synergistic activation of human immunodeficiency virus type 1 promoter activity by NF-κB and inhibitors of deacetylases: potential perspectives*

Integrative Biology Accepted Manuscript

for the development of therapeutic strategies. Journal of virology, 2002. **76**(21): p. 11091-11103.
39. Dar, R.D., et al., *Screening for noise in gene expression identifies drug synergies.* Science, 2014. **344**(6190): p. 1392-1396.
40. Shan, L., et al., *Stimulation of HIV-1-specific cytolytic T lymphocytes facilitates elimination of latent viral reservoir after virus reactivation.* Immunity, 2012. **36**(3): p. 491-501.
41. Burnett, J.C., et al., *Combinatorial latency reactivation for HIV-1 subtypes and variants.* Journal of virology, 2010. **84**(12): p. 5958-5974.
42. Flusberg, D.A. and P.K. Sorger, *Modulating cell-to-cell variability and sensitivity to death ligands by co-drugging.* Physical biology, 2013. **10**(3): p. 035002.
43. Van Lint, C., et al., *Transcriptional activation and chromatin remodeling of the HIV-1 promoter in response to histone acetylation.* The EMBO journal, 1996. **15**(5): p. 1112.
44. Verdin, E., P. Paras Jr, and C. Van Lint, *Chromatin disruption in the promoter of human immunodeficiency virus type 1 during transcriptional activation.* The EMBO journal, 1993. **12**(8): p. 3249.
45. Barboric, M., et al., *NF-κB binds P-TEFb to stimulate transcriptional elongation by RNA polymerase II.* Molecular cell, 2001. **8**(2): p. 327-337.
46. Brown, C.R. and H. Boeger, *Nucleosomal promoter variation generates gene expression noise.* Proceedings of the National Academy of Sciences, 2014. **111**(50): p. 17893-17898.
47. Brown, C.R., et al., *Linking stochastic fluctuations in chromatin structure and gene expression.* PLoS biology, 2013. **11**(8): p. e1001621.
48. Stasevich, T.J., et al., *Regulation of RNA polymerase II activation by histone acetylation in single living cells.* Nature, 2014. **516**(7530): p. 272-275.
49. Chattopadhyay, P.K., et al., *Single-cell technologies for monitoring immune systems.* Nature immunology, 2014. **15**(2): p. 128-135.
50. Satija, R. and A.K. Shalek, *Heterogeneity in immune responses: from populations to single cells.* Trends in immunology, 2014. **35**(5): p. 219-229.
51. Cohen, A.A., et al., *Dynamic proteomics of individual cancer cells in response to a drug.* science, 2008. **322**(5907): p. 1511-1516.

Figures Legends

Figure 1. Design and operation of the passive-flow microfluidic device. (A) Schematic diagram of the microfluidic device fabrication process (see Methods for more detail). (B) Schematic diagram of the protocol to trap single cells in the passive-flow microfluidic device.

Figure 2. Two trap designs at high and low densities were tested for single-cell capture. (A) SEM images of high density (Hd) and low density S and V traps. Scale bar represents 50 μm. (B) Flow simulation results of surface velocity and streamline plots at 300 μm s^{-1}

Integrative Biology Accepted Manuscript

inlet flow velocity. (C) Overlay of bright field and fluorescent images of live cells stained with calcein AM viability dye trapped in the microfluidic device.

Figure 3. Optimization and characterization of the cell-trapping protocol for the Hd-V microfluidic device. (A) Effect of cell loading density on the overall and single-cell trapping efficiency. (B) Effect of loading volume on the overall and single-cell trapping efficiency. (C) Cell retention following a wash step. (D) Cell retention efficiency while imaging cells over a span of 12 hours. (A-D) Data are presented as the mean ± standard deviation of two independent experiments (n=2). (E) Image of a colored dye traveling through the channel at different time points (Scale bar represents 150 μm). (F) Fluorescent image of cell trapping in the device over time. Cells are labeled with calcein AM.

Figure 4. The activation of latent HIV is highly heterogeneous in a Jurkat T cell line latency model. (A) Time lapse images of activation in Jurkat cells upon stimulation with PMA. Scale bar indicates 100 μm. (B) Heat plots of single-cell GFP expression over time quantified from time-lapse images in response to LRA treatment (upper panels). Mean fluorescence intensity (MFI) was plotted over time, and time courses are represented as three-frame running averages to reduce the influence of high-frequency noise. Level of HIV-GFP expression is color-coded on left. Only cells that activated are included. (Lower panel) Data depicted as single-cell activation trajectories. Black line indicates the average trace for each condition. Total % of cells activated by 12 hours is indicated. (C) Correlations between % cells activated in the passive-flow device versus % cells activated in plate-based assay and quantified by flow cytometry. One data point is presented for each treatment at 6 hours (blue triangles), 12 hours (red circles), and ~24 hours (green squares) after stimulation. R indicates Pearson correlation coefficient. Complete data is presented in Fig. S3. (D) Schematic of metrics extracted from individual HIV activation trajectories.

Figure 5. LRAs differentially affect the dynamics latent HIV activation. (A) Distributions (violin plots) of onset time of activation (t_{on}) for only reactivated cells (mean n = 146; range of n is 38-348). White dot indicates mean of distribution. (B) Coefficient of variation (CV) for t_{on} depicted in A. Error bars represent 95% confidence interval obtained by bootstrapping. (C) Distributions of maximum HIV expression (F_{maxO}) for all cells (mean n = 347; range of n is 237-537). (D) CV for F_{maxO}. (E) Distributions for rate of HIV production (S) for all cells. (F) CV for S. Comparison of CVs for metrics calculated from all cells and only activated cells are included in Fig. S6.

Figure 6. Evaluating correlations between metrics of HIV activation in single cells suggests multiple mechanisms control the reversal of latency. (A) Scatter plot depicting the correlation between onset time of activation (t_{on}) and rate of HIV production (slope; S) for cells activated by PMA. R indicates Pearson correlation coefficient. (B) Correlations between t_{on} and S for all perturbations. (C) Examples of correlations

Integrative Biology Accepted Manuscript

between either t_{on} (left) or S (right) and maximum HIV expression (F_{maxO}) in cells activated by PMA. (D) Regression coefficient between t_{on} (blue) or S (red) and F_{maxO} for all perturbations. Regression coefficients were determined using multiple regression analysis. Coefficient of determination (R^2) for each multiple regression is indicated above each bar. Error bars represent 95% confidence intervals.

Integrative Biology Accepted Manuscript

Figure 1

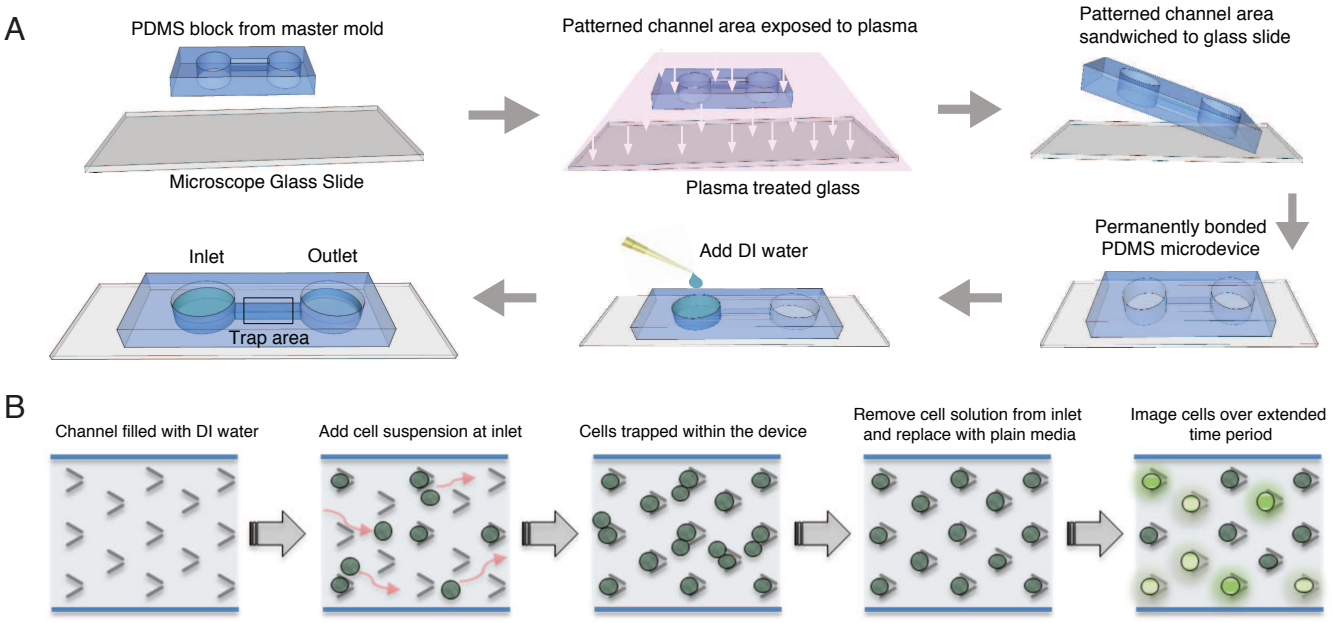

Integrative Biology Accepted Manuscript

Figure 2

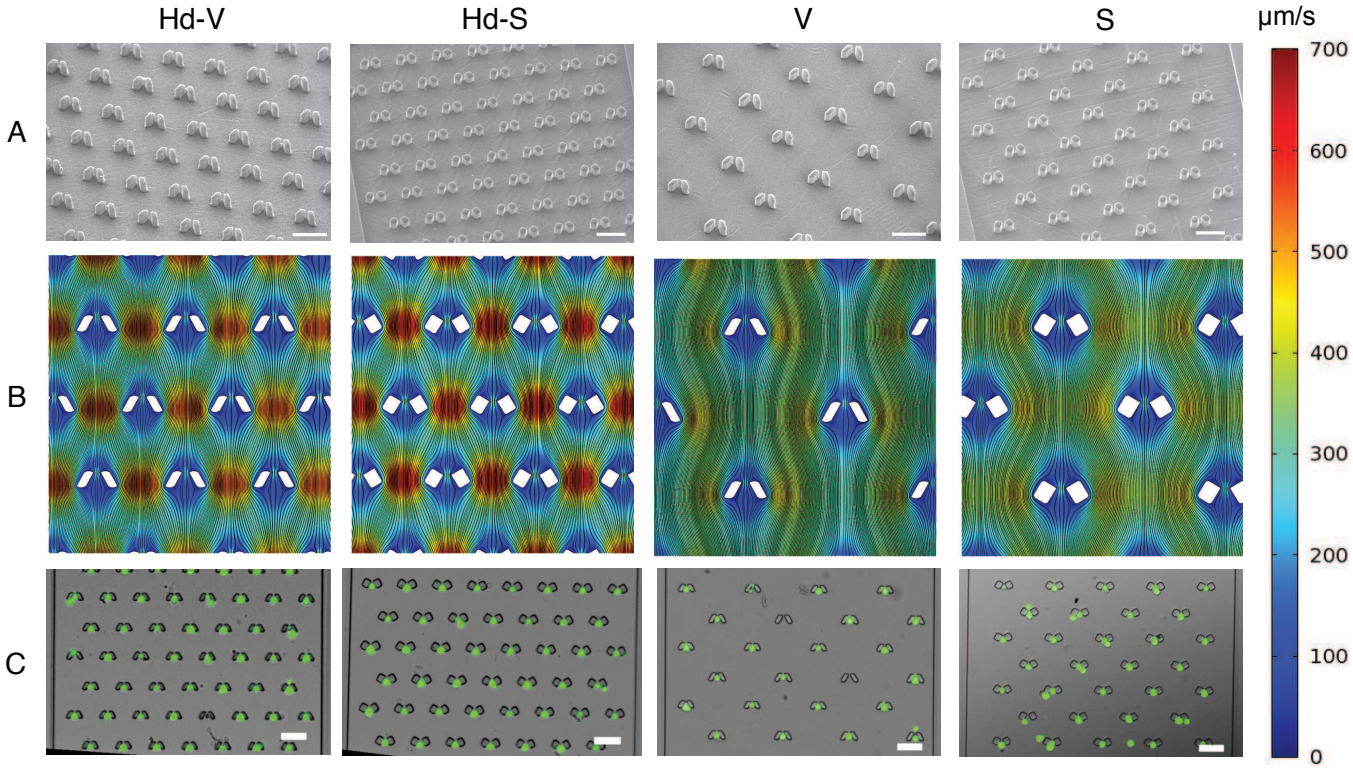

Integrative Biology Accepted Manuscript

Figure 3

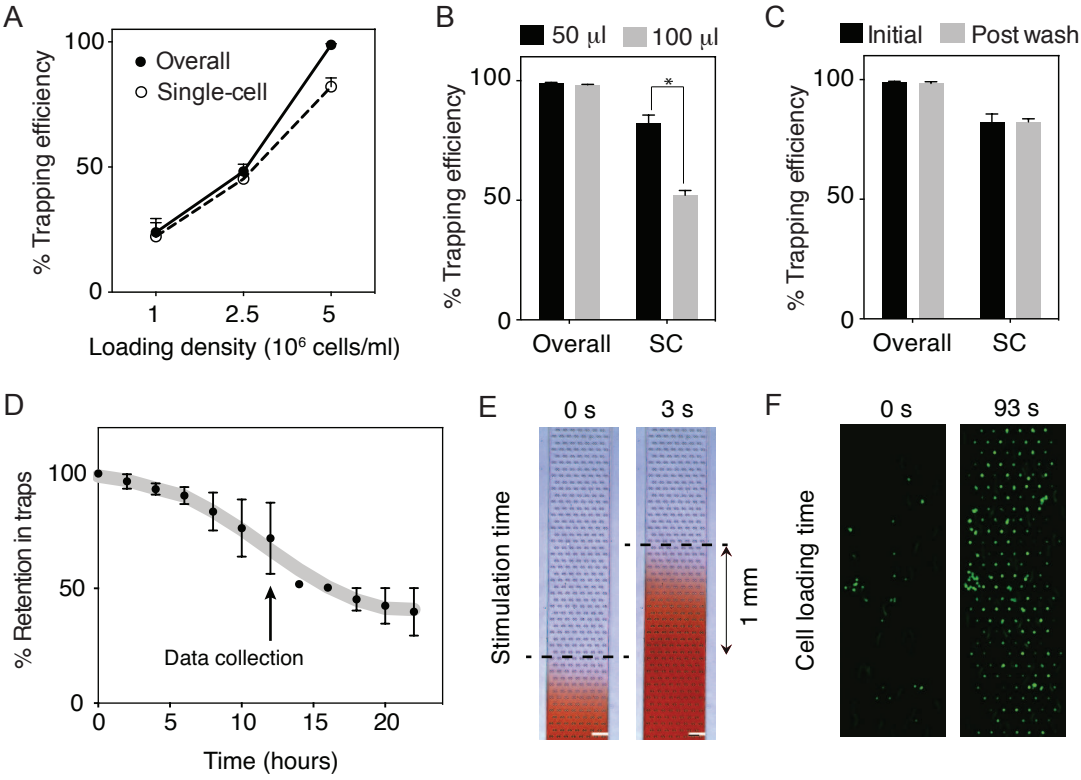

Integrative Biology Accepted Manuscript

Figure 4

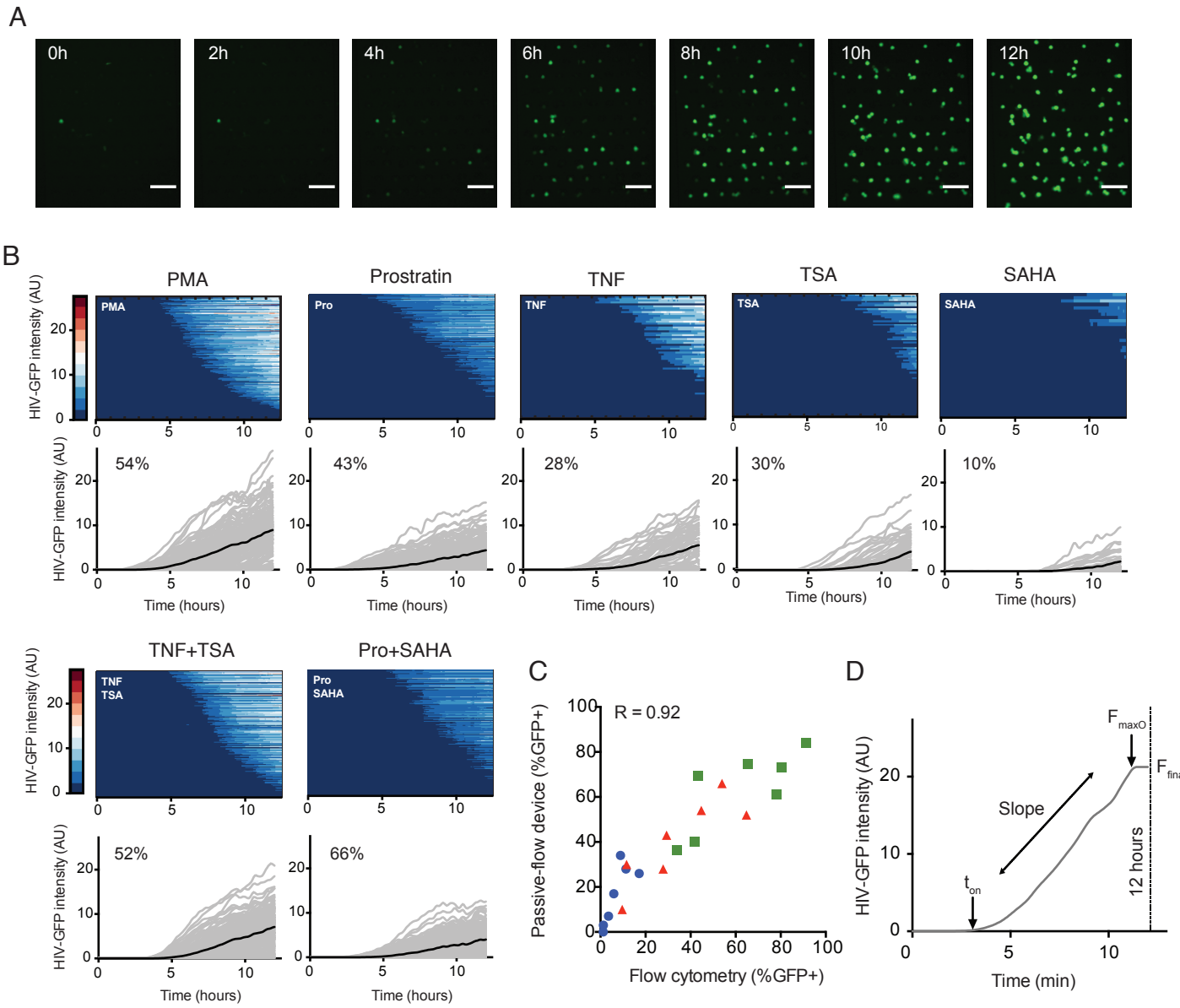

Integrative Biology Accepted Manuscript

Figure 5

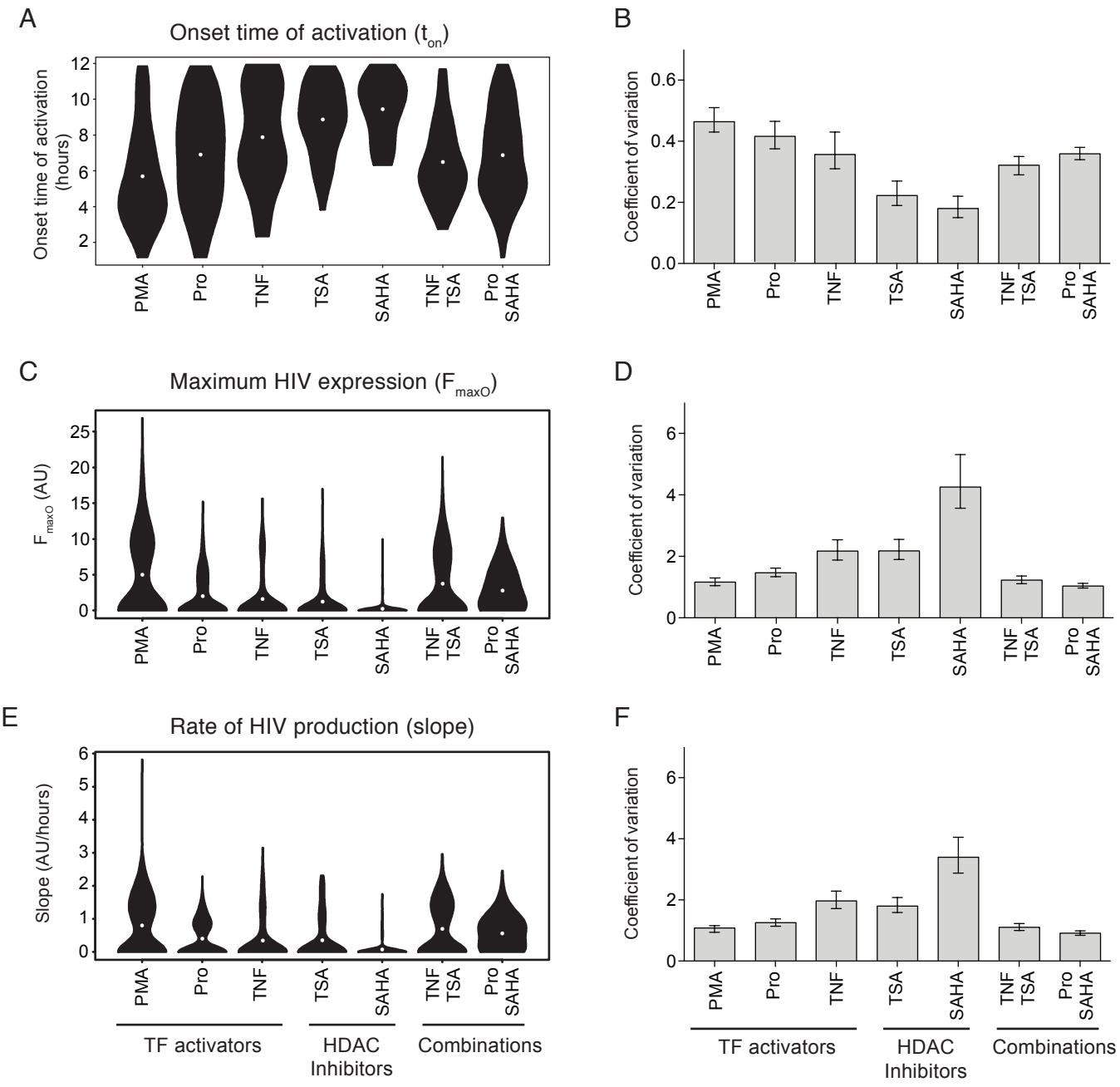

Integrative Biology Accepted Manuscript

Figure 6

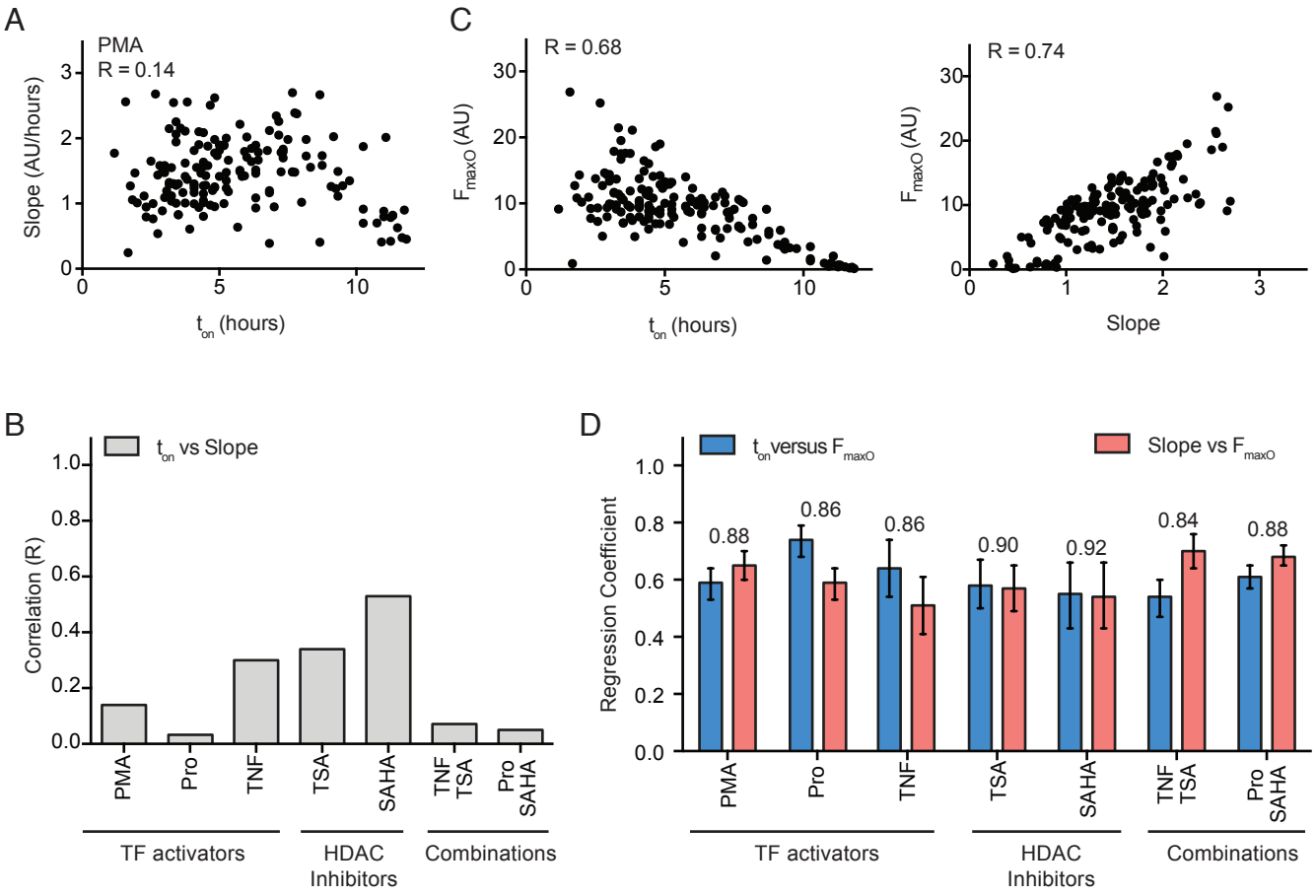

Integrative Biology Accepted Manuscript